Talanta 265 (2023) 124882

Contents lists available at ScienceDirect

Talanta

journal homepage: www.elsevier.com/locate/talanta

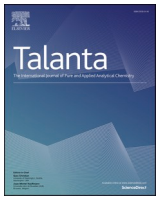

Electrochemical biosensor for aerobic acetate detection

E. Forner [a], J.J. Ezenarro [b], M. Pérez-Montero [c], N. Vigués [b], A. Asensio-Grau [d], A. Andrés [d], J. Mas [b], M. Baeza [e], X. Muñoz-Berbel [a,f], R. Villa [a,f], G. Gabriel [a,f,*]

[a] Institut de Microelectrònica de Barcelona, IMB-CNM (CSIC), Universitat Autònoma de Barcelona, Cerdanyola Del Vallès, 08193, Barcelona, Spain
[b] Department of Genetics and Microbiology, Universitat Autònoma de Barcelona, Cerdanyola Del Vallès, 08193, Barcelona, Spain
[c] Basic Sciences Department. Faculty of Medicine and Health Sciences. Universitat Internacional de Catalunya, 08195, Sant Cugat Del Vallès, Barcelona, Spain
[d] Instituto de Ingenieria de Alimentos para El Desarrollo, Universitat Politècnica de València, Camino de Vera S/n, 46022, València, Spain
[e] GENOCOV Research Group, Department of Chemistry, Faculty of Science, Edifici C-Nord, Universitat Autònoma de Barcelona, Cerdanyola Del Vallès, 08193, Barcelona, Spain
[f] CIBER de Bioingeniería, Biomateriales y Nanomedicina, Instituto de Salud Carlos III, Spain

ARTICLE INFO

Handling Editor: Agata Michalska

Keywords:
Electrochemical biosensor
Inkjet printed sensor
Alginate hydrogel matrix
Reduced graphene oxide
Escherichia coli
Acetate detection

ABSTRACT

There is an increasing demand on alternatives methods to animal testing. Numerous health parameters have been already studied using in vitro devices able to mimic the essential functions of the organs, being the real-time monitoring and response to stimuli their main limitations. Regarding the health of the gut, the short chain fatty acids, and particularly acetate, have emerged as key biomarkers to evaluate gut healthiness and disease development, although the number of acetate biosensors is still very low. This article presents a microbial biosensor based on fully biocompatible materials which is able to detect acetate in aerobic conditions in the range between 11 and 50 mM, and without compromising the viability and function of either bacteria (>90% viability) or mammalian cells (>80% viability). The detection mechanism is based on the metabolism of acetate by *Escherichia coli* bacteria immobilized on the transducer surface. Ferricyanide is used as a redox mediator to transfer electrons from the acetate metabolism in the bacterial cells to the transducer. High bacterial concentrations are immobilized in the transducer surface (10^9 cfu mL^{-1}) by electrodeposition of conductive alginate hydrogels doped with reduced graphene oxide. The results show successful outcomes to exploit bacteria as a biosensing tool, based on the use of inkjet printed transducers, biocompatible materials and cell entrapment technologies.

1. Introduction

The human gut is an active environment in which microorganisms continuously interact with the host via their metabolic products. Among the different microbial metabolic products, the most important ones are the fermentation products such as short chain fatty acids (SCFAs) [1]. The main SCFAs are acetic, butyric, propionic, valeric, isobutyric, and isovaleric acids, being the primary end-products of fermentation of non-digestible carbohydrates.

The SCFAs have a key role in glucose and lipid homeostasis [2], and numerous works evidenced the link between the SCFA with gut inflammation [3] and the control of human metabolic pathways [4]. Therefore, an intestinal bacteria imbalance, which can be assessed by the SCFAs concentration, plays an important role in the development of several disorders such as diabetes [5], Alzheimer's and Parkinson's disease [6], or cardiovascular disease [4], among others. Acetate, propionate and butyrate have been identified in the microbiota-gut interactions leading to diseases [7]. Consequently, the knowledge concerning the paper of these SCFAs is crucial to unravel many aspects of the body's metabolism and the development of pathologies.

The SCFA real-time determination is still challenging. Currently, SCFAs are quantified in blood plasma or serum using bulky benchtop equipment such as gas or liquid chromatography [8], and ion exclusion chromatography [9], which is expensive, complex and time-consuming. Fecal samples are also very common in the study of gut, which require tedious pre-treatments and quantification by the so-called metabolomic technique [10]. So, there is still a lack of commercial sensors able to perform online and real-time measurements of these analytes, in a fast,

* Corresponding author. Institut de Microelectrònica de Barcelona, IMB-CNM (CSIC), Universitat Autònoma de Barcelona, Cerdanyola del Vallès, 08193, Barcelona, Spain.
E-mail address: gemma.gabriel@imb-cnm.csic.es (G. Gabriel).

https://doi.org/10.1016/j.talanta.2023.124882
Received 19 January 2023; Received in revised form 17 June 2023; Accepted 24 June 2023
Available online 8 July 2023

simple and cost-effective manner.

In recent years, colonic in vitro fermentation models as well as the organ-on-chip (OOC) technology has emerged and consolidated. Since studying colonic fermentation in vivo entails several restrictions, colonic in vitro fermentation models are a worthwhile alternative used in the food and health research field [11,12]. The simulation of colonic fermentation in vitro, especially the dynamic models that are used for long-term experiments require the continuous control of microbiota, which is commonly done by sampling and externally measuring the metabolites production, such as SCFAs among others [13]. On the other hand, OOC consists of microfluidic tools that emulate relevant conditions of the in vivo cell microenvironment. Successful examples of OOCs mimicking the tissue- and organ-level physiology and function of brain [14], liver [15], vasculature [16] and gut, have been already developed [17]. Regarding to the latter, Trapecar et al. demonstrated how SCFAs reduce innate inflammation of the ulcerative colitis gut in absence of Treg and Th17 cells by single measures of individual samples collected from the Gut-on-a-Chip (GOC) system [18]. Unfortunately, such structure still missed integrated sensing elements able to monitor SCFAs on-chip.

Few SCFA biosensors have been already reported, which take benefit of the bacterial capacity to metabolize specific SCFA. Most of these microbial biosensors use bacterial biofilms composed of specific bacteria capable to utilise SCFAs as carbon source in anaerobic conditions. This is the case of: (i) the anaerobic microbial fuel cell developed by Kaur et al. in 2013 [19], which was able to quantify SCFA above 80 mg L^{-1} and discriminate between acetate, butyrate and propionate; (ii) the bio-electrolytic sensor presented by Jin et al., able to quantify mixtures of acetate, propionate and butyrate in wastewater over a 5 month period [20] by following the anaerobic digestion of SCFA; and (iii) the miniaturized amperometric microbial microsensors reported by Atci et al., capable to oxidise acetate [21] and lactate [22], and to quantify them in a depth profile inside a biofilm-based glass pipette microsensor. Although very attractive and promising, these sensors rely on the formation of poorly repetitive and heterogeneous bacterial biofilms, the use of specific bacterial types and the need for anaerobic conditions during the measurement, which is difficult to implement in current GOC systems containing gut cells growing aerobically. Recently, Wang et al. demonstrated that acetate can be metabolized in aerobic conditions using the gram-negative bacterium *Escherichia coli* (*E. coli*) and artificial mediators as electron acceptors [23]. This idea may be extended to bioelectrocatalytic systems for the oxidation and measurement of acetate although currently, there is no electrochemical microsensors enabling SCFA measurement in aerobic conditions.

As a step forward in SCFAs detection, we present an amperometric *E. coli* microbial biosensor for long-term monitoring of acetate in aerobic conditions. Specifically, we demonstrate how *E. coli* is able to metabolize acetate by oxidizing it and, thanks to the use of ferricyanide as final electron acceptor, this metabolic oxidation is indirectly measured electrochemically. For the very first time bacteria is immobilized inside a conductive alginate hydrogel over a printed microsensor. The alginate hydrogel acts as a biocompatible 3D scaffolds for cell entrapment, retaining bacteria in a controlled and physiological environment. The doping of the polymeric matrix with reduced graphene oxide (rGO) increases the gel conductivity, achieving the same electrochemical response as the activated bare gold (Au) electrode, one of the best metallic electrodes to our knowledge. The electrochemical microbial biosensor for acetate is envisaged in the future as a promising candidate to be implemented inline at the outlet port of the GOC chamber. This microbiosensor should contribute to unravel the bidirectional interaction between gut cells and microbiota, as well as the mechanisms leading to pathology development, through the analysis of one of the main SCFAs, i.e. acetate.

2. Materials and methods

2.1. Reagents and materials

Alginic acid sodium salt, calcium carbonate ($CaCO_3$), graphite and phosphate buffered saline (PBS) tablets, sodium butyrate and sodium propionate were purchased from Sigma-Aldrich (Darmstadt, Germany). Potassium ferricyanide and potassium ferrocyanide trihydrate were purchased from Acros Organic (Darmstadt, Germany). Glucose and sodium acetate anhydrous for analysis were purchased from Panreac (Barcelona, Spain). All chemicals were used as received. All the solutions were prepared with deionised water. Graphene oxide (GO) was synthesised from flaked graphite (Sigma-Aldrich, St. Louis, MO, USA) using the Hummers' method. Reduced graphene oxide (rGO) was obtained through the reduction of GO using ascorbic acid [24]. A silver (Ag) nanoparticle ink (Dupont-PE410 from DuPont, Delaware, USA), a dielectric photoresist SU-8 ink (SU-8) (Prielex from MicroChem, Massachusetts, USA) and Au colloidal ink (DryCure Au–1010 B from Colloidal Ink Co., Okayama, Japan) were used for the electrodes printing.

2.2. E. coli metabolism and growth experiments

Spectroscopic analysis of *E. coli* bacterial cultures, either turbidimetric or colorimetric, were conducted with a 96-well micro plate reader from Thermo Fisher Scientific (Massachusetts, USA) using the SkanIt Software 2.4.5 for data recording and collection. In turbidity studies, *E. coli* reproduction was monitored at a wavelength of 600 nm for 24–45 h, by taking one measurement every 30 min. Similarly, the metabolic reduction of ferricyanide by *E. coli* was determined colorimetrically by monitoring the decrease in the absorbance magnitude at 420 nm over time, which corresponds to the maximum absorption wavelength of ferricyanide. As before, the measurements were taken every 30 min for a total of 24–45 h. In both cases, the 96-well micro plate was regularly shaken to prevent bacterial sedimentation.

A total of 20 samples, combining five acetate, butyrate and propionate concentrations (i.e. 1.1, 0.88, 0.55, 0.22 and 0 mM) and four glucose concentrations (i.e. 1.1, 0.55, 0.22 and 0 mM), were prepared in minimum medium AB (MMAB) from Sigma-Aldrich (Darmstadt, Germany) to evaluate the capacity of *E. coli* to metabolize acetate in aerobic conditions. Bacterial and ferricyanide concentrations were always set at 10^5 colony forming units per mL (cfu mL^{-1}) and 1 mM, respectively, unless otherwise indicated. Moreover, MMAB alone, MMAB plus glucose, MMAB plus acetate, Luria-Bertani medium (LB) from Sigma-Aldrich (Darmstadt, Germany) without bacteria, and LB plus *E. coli* were studied as control. Three replicas of each condition were prepared and analysed independently.

2.3. Alginate hydrogel formation

Standard three-electrode amperometric sensors were fabricated using Inkjet printing (IJP) technique, as described in detail in the Supplementary Information (SI). Alginate hydrogels were electrodeposited by a modification of the protocol reported in Refs. [25,26]. Briefly, 2 mL of the precursor solution containing alginic acid sodium salt and $CaCO_3$ in deionised water was placed above the working electrode (WE) and electrodeposited at 1.4 V (*vs.* integrated Ag/AgCl pseudo-reference electrode (RE)). The alginic acid concentrations (between 0.1 and 0.75 w/v) and $CaCO_3$ (1% w/v), as well as the electrodeposition time (from 15 to 90 s) were optimized to produce hydrogels with proper uniformity and stability on the electrode. Optimal hydrogels were obtained after 40 s of electrodeposition of precursor solutions containing 0.75% w/v alginic acid sodium salt and 1% w/v $CaCO_3$. After electrodeposition, hydrogels were rinsed to remove residual non-reacted precursor components from the gel. The hydrogel was submerged horizontally into a deionised water full beaker and rinsed carefully until no more waste was

dragged (typically it was rinsed between 4 and 5 times).

2.4. Conductive alginate hydrogel formation

A conducting dopant molecule, either graphite or rGO, was added to the precursor alginate solution before electrodeposition at a concentration of 2% or 4% w/v. In order to guarantee the homogeneity of the precursor solution containing graphite or rGO and to avoid aggregate formation, the solution was sonicated for 5 min with an ultrasound Bandelin Sonoplus HD 3100 from BANDELIN electronic (Berlin, Germany) before electrodeposition. Electrodeposition conditions were the same specificated previously in section 2.3.

2.5. Bacterial conductive alginate hydrogel formation

E. coli suspensions were prepared from the overnight culture as detailed in SI. The overnight culture was centrifuged, and the bacterial pellet was washed and re-suspended in a volume of sterile water that resulted in a bacterial concentration between 10^8 and 10^9 cfu mL^{-1}. The final precursor solution was prepared by mixing 0.4 mL of 4% w/v of alginic acid sodium salt, 0.5 mL of 2% w/v $CaCO_3$, 1.0 mL of deionised water, 2% w/v of rGO and 0.1 mL E. *coli* in a final volume of 2.0 mL. Electrodeposition was conducted at 1.4 V (*vs*. Ag/AgCl pseudo-RE) for 40 s. At these experimental conditions, best hydrogels were obtained when incorporating up to $5{\cdot}10^7$ cfu mL^{-1} in the precursor solution.

2.6. Bacteria viability in electrodeposited conductive alginate hydrogels

The viability of bacteria entrapped in the conductive alginate hydrogels was evaluated using two techniques, i.e. cell counting after plating on agar plates providing the number of viable bacteria in the gel and live/dead staining to see bacterial distribution and viability in the gel.

In the first case, alginate hydrogels were dissolved with 1 mL of 0.1 M PBS, here used as Ca-chelating agent. The resulting solution was sequentially diluted with 0.1 M PBS, and the 1:100, 1:1000 and 1:10,000 dilutions were seeded in agar plates and cultured overnight. The number of viable bacteria were here determined as colonies forming units per mL (cfu mL^{-1}). Plating and counting was conducted in conductive alginate hydrogels containing bacteria just after (t = 0) and 24 h after the electrodeposition. In the case of 24 h of incubation, the hydrogel was stored in the fridge at 5 °C immersed in 1.0 mL of either 0.1 M PBS, 1.1 mM glucose or 1.1 mM acetate.

In a second approach, electrodeposited hydrogels were directly imaged with a confocal microscope (Leica TCP SP5; Wetzlar, Germany) after staining with the Live/Dead Invitrogen Kit BacLight from Molecular Probes (Leiden, Netherlands) as indicated by the supplier. The conductive alginate hydrogel was submerged in 100 μL of Live/Dead staining solution for 15 min, rinsed with water and imaged at an excitation wavelength of 470 nm. Living bacteria stained with SYTO9 appeared green, while dead bacteria stained with propidium iodide appeared in red in the image. The software IMARIS was used for image reconstruction and analysis.

2.7. Cytotoxicity and bactericidal activity of sensor materials and technologies

Optical density measurements at 600 nm were performed to study the toxicity of the materials in contact with bacteria, namely Au (from the WE area) and SU-8 (from the passivation layer). Three different square areas (1 mm^2, 4 mm^2 and 9 mm^2) were printed, and introduced in wells from a 96-wells plate already containing 200 μL of $5{\cdot}10^4$ cfu mL^{-1} *E. coli* in LB medium. Optical density at 600 nm was monitored for 17 h, acquiring values every 30 min. The well plate was shaken before the measurement. All the assay was conducted at 37 °C.

Materials cytotoxicity was determined in the human fibroblast cell line MRC-5 (ATCC Line Bank, Virginia, USA) by using the colorimetric MTT (3-(4,5-dimethylthiazol-2-yl)-2,5-diphenyltetrazolium bromide) assay. Briefly, MRC-5 were seeded in a P24 plate at a density of 80,000 cells mL^{-1} in Dulbecco's modified eagle's medium (DMEM) supplemented with 10% fetal bovine serum and 1% penicillin-streptomycin antibiotic. 24 h after the seed, the tested materials were added into the wells: polyethylene terephthalate (PET), Au and SU-8 (PET was added single dimension 1 mm^2, Au and SU-8 were added in three different dimensions: 1, 4 and 9 mm^2). 72 h after the material addition, the MTT solution (5 mg mL^{-1}) was added and incubated for 1 h (37 °C, 5% CO_2). The purple formazan generated by MTT metabolism of viable cells was solubilised with dimethyl sulfoxide (DMSO). The optical density of each well was determined at 570 nm in a spectrophotometer reader (BioTek® Synergy HT, Vermont, USA). Cell viability was expressed as percentage in relation to non-treated cells. Pictures were taken 72 h after material addition.

2.8. Electrochemical characterisation

CVs were performed in equimolar solutions of ferro/ferricyanide (10 mM) scanning between −0.2 V and 0.5 V at a scan rate of 25 mV s^{-1}. Chronoamperometry was employed to indirectly determine metabolic acetate oxidation, and hence acetate concentration, using ferricyanide as redox mediator. First, *E. coli* microbial modified sensor described in section 2.7 was incubated with a 3 M KCl solution containing acetate and 10 mM ferricyanide for 10 min. Along this time, bacteria oxidized acetate generating an electron flow through the electron transfer chain, resulting in the metabolic reduction of ferricyanide to ferrocyanide, which used as final electron acceptor. Ferrocyanide concentration, which is proportional to acetate, was determined chronoamperometrically by applying a potential of 0.4 V (*vs*. Ag/AgCl pseudo-RE) for 120 s. The experiments, lasting from 6 to 16 h, were conducted at room temperature and with five different acetate concentrations (1.1 mM, 5.5 mM, 11 mM, 20 mM, 30 mM, 35 mM, 40 mM, 50 mM and 60 mM). The same protocol was used to evaluate the metabolic degradation of glucose (1.1 mM), which was used as positive control. Samples obtained from in vitro colonic fermentation (described in section 2.10) of two different subjects were assessed using the above mentioned protocol. Additionally, the nutritional medium PDNM002B was studied. The experiment was carried out at room temperature for a duration of 30 h.

2.9. Morphological characterisation

The thickness of the conductive alginate hydrogel was measured with a confocal microscope PLμ NEOX Sensofar (Terrassa, Spain) and images were treated with Software sensoVIEW1.7.0. A Scanning Electron Microscope (SEM) QUANTA FEI 200 FEG-ESEM with low vacuum (LV) manner in ambient mode was used to acquire images of *E. coli,* calcium alginate, rGO, calcium alginate hydrogels doped with rGO and with rGO and *E. coli*. Elemental analysis of the samples was done with the X-ray diffraction (EDX) module coupled to the previous SEM at random positions of the sample. Alginate hydrogels were also analysed by infrared spectroscopy (IR) with a Bruker Tensor 27 equipment (Madrid, Spain) controlled by Opus 5.5 software.

2.10. In vitro colonic fermentation

The simulation of the colonic fermentation was conducted using a dynamic in vitro model: Simulator of the Human Intestinal Microbial Ecosystem (SHIME®). A triple-SHIME® configuration was set to carry out the experiment, which allows for reproducing colonic fermentation of three subjects, with one colon region each (proximal) simultaneously. The three-SHIME setting consisted of six double-jacketed vessels simulating: (1) the stomach-duodenum and (2) the proximal colon (PC). The vessels were continuously agitated with a magnetic stirrer and warmed to 37 °C. Nitrogen flow kept the anaerobic environment in the vessels

(30 min/day) and the pH was automatically adjusted with the addition of NaCl (0.5 N) and HCl (0.5 N) [27]. Proximal compartments of the colon were filled with 500 mL of nutritional medium, respectively. The stomach and intestinal conditions as well as the pancreatic juice (6 g L^{-1} Oxgall, 12.5 g L^{-1} $NaHCO_3$ and 0.9 g L^{-1} of pancreatin) were simulated as previously described [28].

Prior the experiment, faecal inoculums from fresh faecal samples belonging to three volunteer subjects (mean age 8 years old) were obtained. Faecal samples (40 g) from each subject were fresh collected and kept in refrigeration at 8 °C and anaerobiosis conditions with the use of anaerobiosis bags (Thermo Scientific™ Oxoid AnaeroGen). Samples were processed in a period of less than 4 h before the experiment. First, each faecal sample was mixed in anaerobic phosphate buffer in 20% (w/v) proportion and homogenised for 10 min in a Stomacher. The resulting mixture was poured into a 50 mL falcon tube and centrifuged during 2 min at 500 g-force. Then, the three supernatants were collected and considered as the three different faecal inoculums, from which 5 mL per 100 mL of the volume of nutritional medium were inoculated in the proximal colon bioreactors.

The experiment consisted on four stages over 8 weeks of duration: 1) stabilisation of the microbiota (2 weeks); 2) control period; 3) treatment (2 weeks) including the supplementation of the probiotic (Bifidobacterium animalis $2{\cdot}10^9$ cfu mL^{-1}) to the proximal bioreactors; 4) post-treatment (1 more week) with the same conditions as in the control period (without supplying the probiotic). The nutritional medium PDNM002B was acquired from Prodigest® (Gent, Belgium). Samples from proximal vessels were collected at 14 days after the start of the treatment period, and were stored at −20 °C until the chromatography analysis.

2.11. Analysis of short-chain fatty acids by chromatography

SCFAs were analysed from aliquots taken after 14 days of treatment in a Dionex 3000 ultimate high-performance liquid chromatography (HPLC) (Dionex, Sunnyvale, CA, USA) using a UV detector at 210 nm. The chromatographic separation was performed in an ICE-COREGEL 87H3 column (7.8 × 300 mm, Transgenomic, Omaha, NE, USA), heated at 40 °C, employing 0.006 mM of H_2SO_4 as a mobile phase at a flow rate of 0.5 mL min^{-1}. Samples were filtered at 0.22 μm (Millipore, Burlington, MA, USA).

3. Results & discussion

3.1. General concept: E. coli acetate metabolism

In aerobic conditions, *E. coli* bacteria employ glucose as main carbon source for their proliferation [29,30]. However, other carbon sources based on glucose derivatives, such as acetate, can be also used, with the drawback of presenting lower metabolic efficiencies [23]. For this reason, the metabolic efficiency of two carbon sources, i.e. glucose and acetate, was evaluated by monitoring the changes in the optical density magnitude at a wavelength of 600 nm (OD_{600}) over the proliferation time, this parameter being directly proportional to bacterial concentration. *E. coli* suspensions containing 10^5 cfu mL^{-1} were prepared in MMAB to observe the influence of the carbon source without the interference of other nutrients normally present in rich media. Fig. 1a shows the variation of the OD_{600} over time for the 21 experimental conditions studied combining different glucose and acetate concentrations: (a1) LB medium, used as control, (a2) 1.1 mM glucose, (a3) 0.55

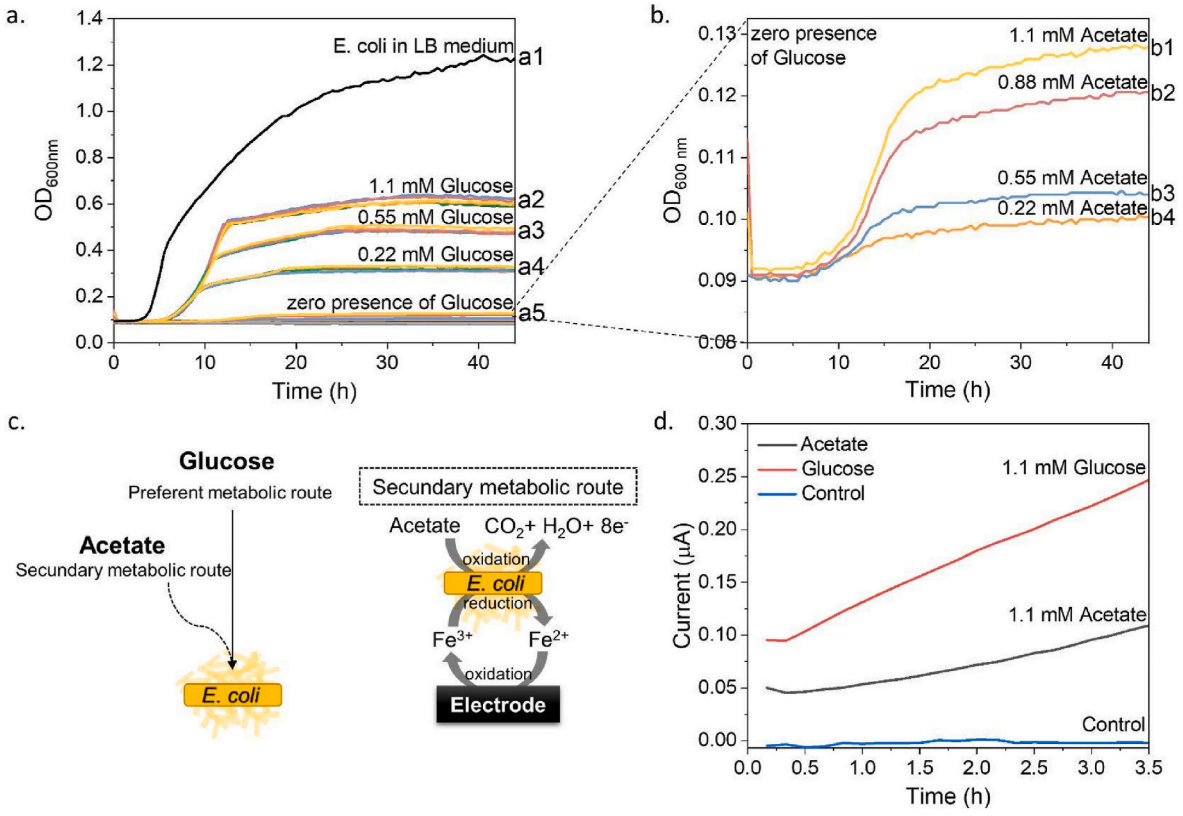

Fig. 1. Determination of *E. coli* growth by taking the absorbance at 600 nm (n = 3) in a) normal LB medium (a1) and cultivated in MMAB and different glucose concentrations 0.11 mM (a2), 0.55 mM (a3), 0.22 mM (a4) and 0.0 mM (a5); and (b) detailed plot of the culture with zero glucose concentration and different acetate concentrations 1.1 mM (b1), 0.88 mM (b2), 0.55 mM (b3) and 0.22 mM (b4). (c) Left: Schematic path of *E. coli* metabolism detailing how *E. coli* metabolises glucose as preferent analyte, and secondly the acetate. Right: Sensing mechanism of the proposed acetate electrochemical biosensor in the presence of the ferrocyanide as mediator. (d) Current response dependency of a *E. coli* suspension at 0.4 V in the presence of 1.1 mM acetate or 1.1 mM glucose, the control was performed with the same current measuring set up with the mediator specimen 10 mM ferricyanide.

mM glucose, (a4) 0.22 mM glucose and (a5) 0.0 mM glucose in MMAB. Each glucose concentration was split into five aliquots, each one supplemented with a different acetate concentration: 0.0 mM, 0.22 mM, 0.55 mM, 0.88 mM and 1.1 mM acetate. The detailed proportions of glucose and acetate, along with their corresponding concentrations for all the tested conditions, can be found in Table S1 in the SI. The acetate concentrations were selected considering the values reported by SCFAs in the circulatory system of human subjects [31].

Control sample a1 presented standard proliferation curves [32], with an exponential growth (log phase) after 2 h of lag phase, and a stationary phase after 20–24 h of proliferation. When the proliferation was conducted in MMAB instead of the rich LB medium, the lag phase was expanded from 2 to 5 h due to a slower proliferation associated to nutrients restriction. Two different regions were observed in the log phase of bacteria proliferating in MMAB containing glucose and acetate: a first one with a slope of 0.040 ± 0.008 A U. minute^{-1} and a second one with a smaller slope of 0.007 ± 0.001 A U. minute^{-1}. Samples only containing acetate as carbon source, i.e. a5 sample, presented a log phase with a single exponential increase. The slope magnitude in a5 coincided with that reported for the second log phase region in a2 to a4 samples. Based on these observations, the two regions in the log phase were associated to different nutrient source. That is, *E. coli* first metabolized glucose, the most efficient and energetic nutrient, resulting in short duplication times (i.e. 160 min) and large slopes in the growing curve. Once glucose was fully consumed, bacteria started to use acetate as carbon source. Since less efficient, acetate metabolism resulted in smaller slopes and longer duplication times of 2000 min. Moreover, the absence of glucose also enlarged the lag phase, which expanded to almost 10 h due to the increase in the time necessary to reach the minimal bacterial concentration detectable by the spectroscopic system.

Even though the oxidation path of acetate was less energetic, an increase of OD_{600} was clearly appreciated, demonstrating that *E. coli* used acetate as carbon source in aerobic conditions. As shown in Fig. 1b for a5 samples, the slope in the log phase of the growth curve was directly proportional to the initial acetate concentration in the MMAB. This behaviour was equally repeated with samples also containing glucose (the detailed plot of each glucose concentration for each acetate mixtures are presented in the, which confirmed the correlation between bacterial metabolism and acetate concentration.

As *E. coli* is known to have a versatile metabolic capacity and can utilise a variety of carbon sources for energy production and growth, its ability to metabolize the other two most common SCFA was studied. To have a more comprehensive understanding of the selectivity of *E. coli* in metabolising propionate and butyrate, the same growth experiments were undergone under the same above conditions. As depicted in Fig. S2 the control samples in LB medium (highlighted in green) exhibit a typical proliferation curve characterized by exponential growth followed by a stationary phase. However, when the proliferation was carried out in MMAB medium instead of the nutrient-rich LB medium with the presence of the corresponding proportions of glucose-butyrate (S2. a) or glucose-propionate (S2. b), we observed only one lag phase of bacterial growth in all cases with glucose. Notably, the duration of the lag phase was directly proportional to the concentration of glucose present in the medium. Contrary, in the absence of glucose, *E. coli* failed to exhibit any growth over the duration of the 25-h experiment, indicating its inability to metabolize either butyrate or propionate. Therefore, we can state that acetate is generally a preferred carbon source for *E. coli* and the bacteria can not efficiently metabolize the butyrate and propionate SCFAs, proving the selectivity of our sensor to acetate.

Acetate metabolism, involving the oxidation of acetate to CO_2 and the generation of an electron flow of 8 electrons per molecule (Fig. 1c) [23], can be monitored using metabolic indicators such as ferricyanide [33]. Due to its low redox potential, ferricyanide is susceptible to react with the electron transport chain components, which metabolically reduces it to ferrocyanide. Ferrocyanide production over time is directly proportional to the metabolic activity of the microorganism, which can be monitored amperometrically [26] or colorimetrically [34] through the reduction of the yellow-coloured ferricyanide to colourless ferrocyanide. Based on the latter, a second metabolic assay was performed where previous a1 to a5 samples were supplemented with 1 mM ferricyanide used as metabolic indicator. In this case, colour changes associated to ferricyanide reduction to ferrocyanide were determined spectroscopically by monitoring the absorbance magnitude at a wavelength of 420 nm, which corresponds to the maximum absorption peak of ferricyanide. As shown in the SI (Fig. S3), both glucose and acetate metabolism resulted in ferricyanide reduction and the complete change of colour of the solution. The monitoring of bacterial metabolism using ferricyanide absorbance instead of OD_{600} was advantageous by two reasons. On the one hand, ferricyanide increased the sensitivity in the detection of bacterial metabolism since colour changes could be detected earlier than bacterial scattering (10 h *vs.* 8 h 30 min in the case of acetate samples). On the other hand, ferricyanide reduction could be detected amperometrically with simple, fast, inexpensive and miniaturized electrochemical instrumentation.

Considering the previous results, a first proof of concept of the electrochemical sensing of acetate metabolism in aerobic conditions was performed using the printed sensors and the custom-made system detailed in the SI and Fig. S4. Experimentally, 200 μL of a bacterial suspension containing 10^8 cfu mL^{-1} *E. coli* in MMAB supplemented with 1 mM ferricyanide and either 1.1 mM glucose or 1.1 mM acetate as carbon source were prepared and deposited on the electrode surface. Ferrocyanide production was monitored for 3 h and 30 min by chronoamperometry. The chronoamperometric measurement consisted of applying 0.4 V at IJP-WE (*vs.* Ag/AgCl pseudo-RE) for 120 s every 10 min, for the duration of the experiment. Results, illustrated in Fig. 1d, showed a progressive increase in the current magnitude over time resulting from the accumulation of ferrocyanide in the system due to the *E. coli* metabolic activity. As expected, the increase in current value was more accentuated with glucose than when using acetate as carbon source. This fact was associated to the higher metabolic efficiency of glucose, resulting in higher ferrocyanide concentrations and larger intensity values over time. However, *E. coli* metabolism of acetate in aerobic conditions could be monitored amperometrically when employing ferricyanide as metabolic indicator, which validated the detection principle.

3.2. Electro-addressable conductive alginate hydrogels for bacterial entrapment

Inline acetate monitoring in GOC microfluidic devices using metabolic sensors requires the encapsulation of high concentrations of living bacteria to avoid their physical contact with gut mammalian cells. Alginate hydrogels were selected for enabling electrodeposition at soft environmental conditions (i.e. pH = 7, room temperature, aqueous solutions), and providing high control of the electrodeposited area and the thickness of the gel [25]. The electrodeposition process was based on the use of two precursor solutions, one containing $CaCO_3$ and another with alginic acid sodium salt. The application of high potentials on the electrode surface (i.e. 1.4 V *vs.* Ag/AgCl RE) produced water splitting and the local formation of protons. Protons dissolved $CaCO_3$ particles releasing calcium cations that acted as cross-linkers of the alginate monomers and induced the formation of the alginate hydrogel matrix. This strategy has been already used in bacterial entrapment [26], where high bacterial concentrations were immobilized in alginate hydrogels without compromising their viability (>90% viability after electrodeposition) and metabolic capacity, even when doping the gels with conductive graphite particles.

Based on that, alginate hydrogel electrodeposition was optimized considering three aspects: alginate hydrogels electrodeposition, doping of the precursor solutions to produce conductive hydrogels and bacterial entrapment (Fig. 2a).

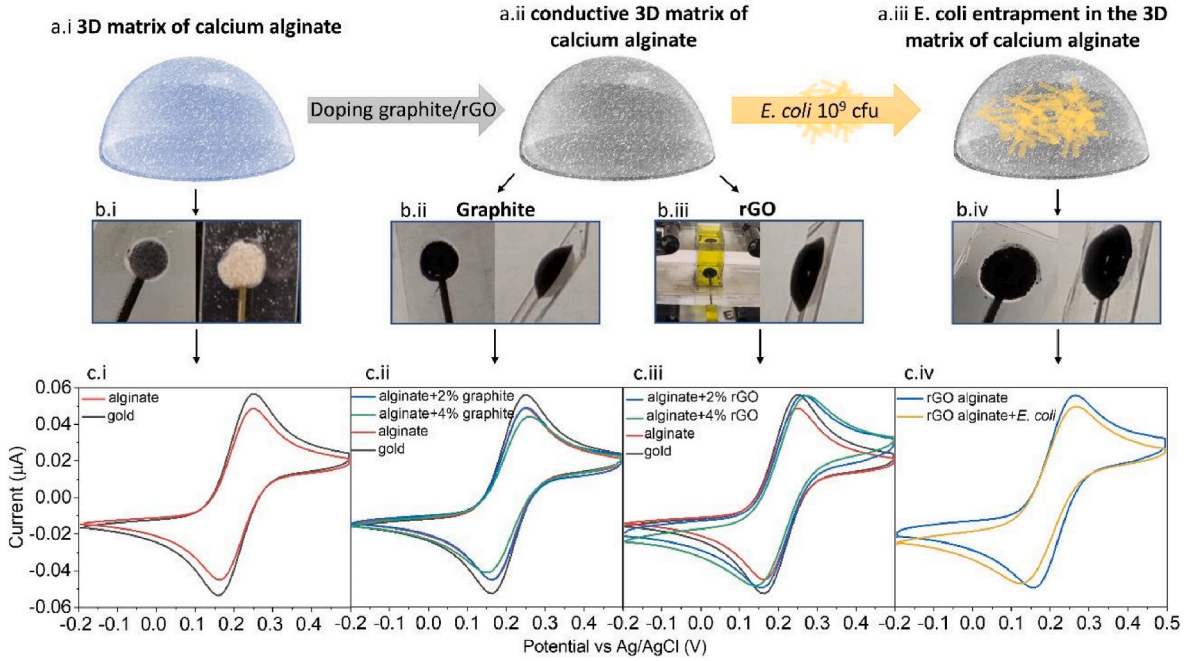

Fig. 2. (a) Scheme of the preparation steps of alginate hydrogel (a.i), conductive alginate hydrogel (a.ii) and *E. coli* entrapment (a.iii). (b) Pictures and (c) CVs comparison of alginate hydrogel (i), dopped alginate hydrogel with graphite (ii), dopped alginate hydrogel with rGO (iii), and with 10^9 cfu *E. coli* (iv). All CVs were performed at 25 mV s^{-1} with an equimolar mixture of ferri/ferrocyanide 10 mM under standard laboratory conditions using 2 mm diameter IJP-WE.

3.2.1. Electrodeposition of alginate hydrogels

Alginate hydrogels were optimized in terms of composition of the precursor solution and electrodeposition time employing 1 mm and 2 mm IJP-WE Au electrodes (details in Table S2 in the SI section). As a result, none of the conditions studied produced stable hydrogels on the 1 mm WE diameter electrodes, independently on the electrodeposition time and the composition of the precursor solution. As shown in Fig. S5 in the SI section, thin alginate hydrogels dried very quickly, while thicker ones detached from the electrode surface due to the small area of the electrode. Bigger 2 mm electrodes provided more reaction points for the electrostatic interaction between the functional groups in alginate and the Au, resulting in the formation of hydrogels that were stably attached to the electrode surface. Optimal conditions involved the electrodeposition at 1.4 V (*vs.* Ag/AgCl RE) of precursor solutions containing 1% (w/v) of alginic sodium salt and 0.75% (w/v) of $CaCO_3$ concentrations (Fig. 2b i). The presence of the alginate hydrogel reduced the electrochemical response of the sensor. Hence, the alginate-modified electrodes presented anodic currents for equimolar mixtures of ferri/ferrocyanide (10 mM) that were 0.85-fold smaller than those obtained with Au bare electrodes. This decrease was associated to the non-

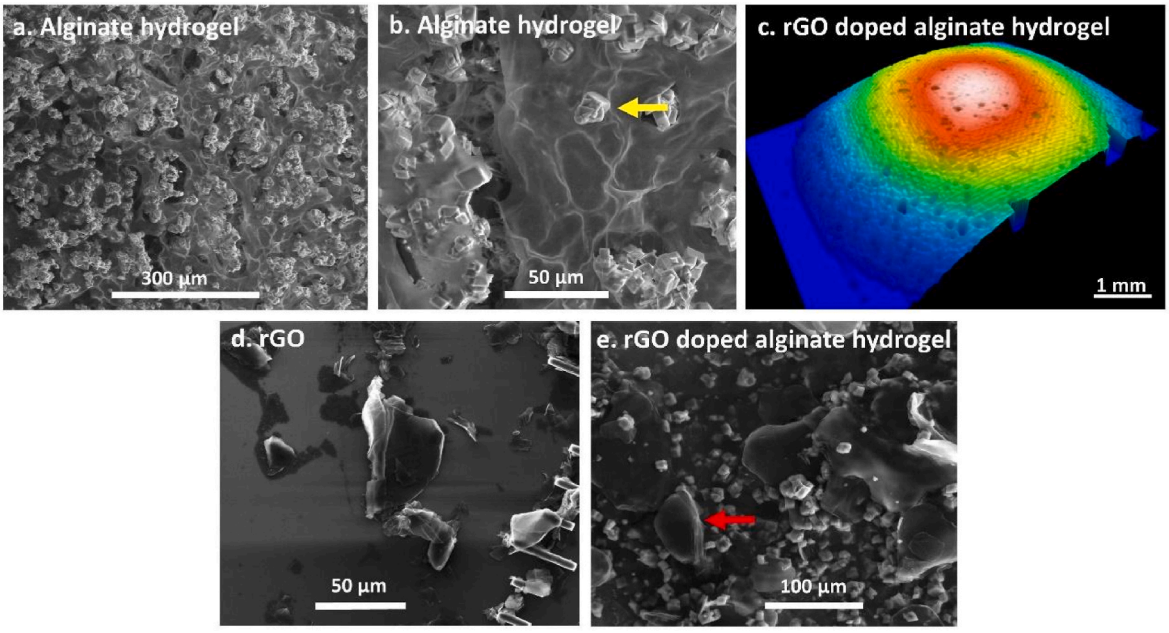

Fig. 3. LV-SEM images of alginate hydrogel (a) and (b) at different magnifications. Yellow arrow points $CaCO_3$ crystals. (c) Confocal microscope image of the semi-sphere shape of 2% w/v rGO doped calcium alginate hydrogel over the IJP WE electrode. LV-SEM images of (d) rGO and e) 2% w/v rGO doped calcium alginate hydrogel. Red arrow points rGO flakes.

conducting porous nature of the hydrogel. In Fig. 3a, LV-SEM images of alginate hydrogels show the high porosity of this matrix, which associated to its cross-linked configuration. $CaCO_3$, precipitated as single cube crystals and identified by EDX analysis (Fig. S6 in SI), were also clearly observed in the alginate matrix in Fig. 3b (pointed with a yellow arrow).

3.2.2. Conductive alginate hydrogels

In order to minimize their electrical isolation, alginate hydrogels were dopped with two conductive materials, graphite and rGO, each one implemented in the precursor solution at two different concentrations, i.e. 2 % and 4% w/v (Fig. 2a ii) [26]. The uniformity of the conductive alginate hydrogels strongly depended on the suitable homogenisation of the precursor solution, which achieved after 5 min sonication at 30% of amplitude. The electrodeposition of homogeneous precursor solutions produced conductive hydrogels on the electrode surface, which completely black due to the presence of the dopant (Fig. 2b ii and 2 b.iii). Conductive alginate hydrogels based on graphite were unstable, detaching from the electrode few hours after the electrodeposition. This low interaction between the gel and the electrode also affected their electrochemical response, providing anodic currents not significantly different of those reported by non-dopped alginate hydrogels (Fig. 2c ii). In opposition, gels dopped with rGO presented longer stabilities of several days and current values similar to those provided by the activated bare electrode (Fig. 2c iii). Since both 2% and 4% w/v rGO precursor solutions showed significantly similar stabilities and electrochemical responses, the 2% w/v was chosen to minimize the use of reagents and the possible negative effect of rGO molecules on bacterial trapping and viability. Fig. 2c clearly shows a lack of effect of the presence of the hydrogel on the shape and intensity of the current signal of the redox probe. This has been previously described by Márquez et al. who investigated the diffusion time of ferricyanide through this same alginate hydrogel proving that the saturation time was reached after 2 min [25]. This fact can be understood as alginate hydrogel is a very porous structure with a high water content, which allows for fast diffusion of species within the gel. This fast diffusion helps to minimize any potential limitations on electron transfer processes. In our work, the addition of reduced graphene oxide (rGO) to the alginate hydrogel improves its electrical conductivity facilitating even more the efficient transfer of electrons between the redox probe and the electrode surface.

The 2% w/v rGO doped calcium alginate hydrogels were characterized by microscopy and IR. Confocal microscopy analysis confirmed the formation of thick and repetitive conductive 3D hydrogels matrix with a thickness of 150 ± 35 μm (Fig. 3c). SEM images showed the presence of rGO as flakes of several microns (Fig. 3d) entrapped inside the hydrogel (Fig. 3e; pointed with a red arrow). The incorporation of rGO inside was due to entrapment, and did not involve the formation of additional bonds, as confirmed by IR. IR spectra corresponding to non-conductive and conductive hydrogels are presented in Fig. S7b in SI, showing identical peaks at 1714 cm^{-1} (corresponding to C═O stretching of carboxylic groups) and in the range between 1300 and 1000 cm^{-1} associated to C–*O*–C and C–OH stretching bonds. All these peaks matched with the chemical structure of calcium alginate (Fig. S7c in SI). Additionally, the alginate hydrogel with 2% w/v rGO presented long-term stability when stored wet and in the fridge (4 °C), providing identical electrochemical responses within 3 days (Fig. S7a in SI). After 3 days, the hydrogels dried losing consistency and electrochemical response, although maintaining high adherence to the electrode.

3.2.3. Bacterial entrapment on conductive alginate hydrogels for biosensing

For biosensing, 0.1 mL of bacteria suspensions between 10^8 and 10^{11} cfu mL^{-1} were introduced to the precursor solution and electrodeposited following the previous protocol. Experimentally, it was not possible to produce alginate hydrogels through water splitting when using bacterial suspensions above $1{\cdot}10^9$ cfu mL^{-1}. Below that concentration, stable alginate hydrogels were generated on the electrode surface, which presented suitable adherence, consistency and an appearance similar to those non-containing bacteria (Fig. 2b iv). LV-SEM images of these conductive alginate hydrogels (Fig. 4a) show bacteria inside the gel, which presented the conventional rod morphology, with a length of 1.08 ± 0.07 μm and a width of 569 ± 127 nm. The *E. coli* immobilized inside the 3D-porous structure of the conductive alginate hydrogel were in contact with rGO, $CaCO_3$ and alginic acid sodium salt, and bacteria were also observed on $CaCO_3$ crystals (in Fig. 4b, pointed with a yellow arrow).

Live and dead bacteria tests were conducted to verify that the material and the electrodeposition procedure were nonthreatening for *E. coli* (Fig. 4c). To this end, conductive alginate hydrogels were dissolved in 0.1 M PBS right after *E. coli* immobilization, and stained with Live/Dead Invitrogen Kit BacLight. The samples were then imaged with a confocal microscope, where live bacteria appeared in green and dead ones in red. According to the results, 77 ± 7% of the encapsulated bacteria were alive, while only the 26 ± 7% were dead (n = 6). These values coincided with those obtained with the culture before encapsulation, which confirmed that the electrodeposition procedure did not compromise cell viability.

Additionally, since the sensor was expected to monitor acetate for long-term periods, it was necessary to study the *E. coli* survival inside the alginate hydrogels. To accomplish it, *E. coli* bacteria immobilized inside the D semi-sphere structure was quantified after gel resuspension, plating and counting. Freshly prepared conductive alginate hydrogels were considered as references and compared with samples stored for 24 h in different media: 1 mL of 0.1 M PBS, 1 mL of 1.1 mM glucose and 1 mL of 1.1 mM acetate. The number of live bacteria just after electrodeposition (t = 0 h) of a hydrogel from WE, i.e. $8.0{\cdot}10^9$ cfu gel^{-1}, was reduced one magnitude order after 24 h of storage in PBS ($3{\cdot}10^8$ cfu gel^{-1}) and two magnitude orders when stored in glucose ($2.1{\cdot}10^7$ cfu gel^{-1}) or acetate samples ($4.8{\cdot}10^7$ cfu gel^{-1}). The lower ionic conductivity and the lower control of the pH of the glucose and acetate solutions, less physiologic than PBS, resulted thus in a higher bacterial mortality than in PBS. However, the death rate in all cases was in agreement with the results obtained in solution, confirming the biocompatibility (and low toxicity) of the materials and electrodeposition protocols employed for the hydrogel formation, and their stability inside the gels.

On the other hand, the influence of the electrode materials in the metabolic activity of *E. coli* and their toxicity was also evaluated. Toxicity test consisted of the analysis of bacterial proliferation in LB media alone, and in the presence of printed Au and SU-8 PET samples with areas of 1, 4 and 9 mm^2. The OD_{600} of the samples was measured for 17 h (Fig. 4e), and the growth rate and the bacterial generation (determined as duplication time, DT) were determined from the exponential growth phase for each condition. The DT is defined as the time necessary by a bacterial population to duplicate (DT = ln2/μ). It is directly proportional to the growth rate constant, μ, which depends on the growth line defined as:

$$N_t = N_0 \exp .^{\mu(t-t0)} \quad (1)$$

where N is the bacterial concentration and t is the time.

The analysis of the previous experimental conditions showed a DT between 30 and 40 min for *E. coli*, which coincided with reported values by this bacterial strain [35], demonstrating that inkjet-printed Au and SU-8 were not affecting bacterial viability or proliferation. Therefore, the electrodeposition process, the materials and IJP technologies involved in the sensor fabrication were harmless for bacterial entrapment and may be used in the development of microbial biosensor in self assembled IJP electrodes.

Finally, and considering the implementation of the sensor, the cytotoxicity of the sensor materials and fabrication technologies was evaluated using human fibroblast cell line MRC-5 as model mammalian cell line. To the best of our knowledge, this study is the first one to report on the cytotoxic effect on human cells of IJP inks. In this case, 1, 2 and 3

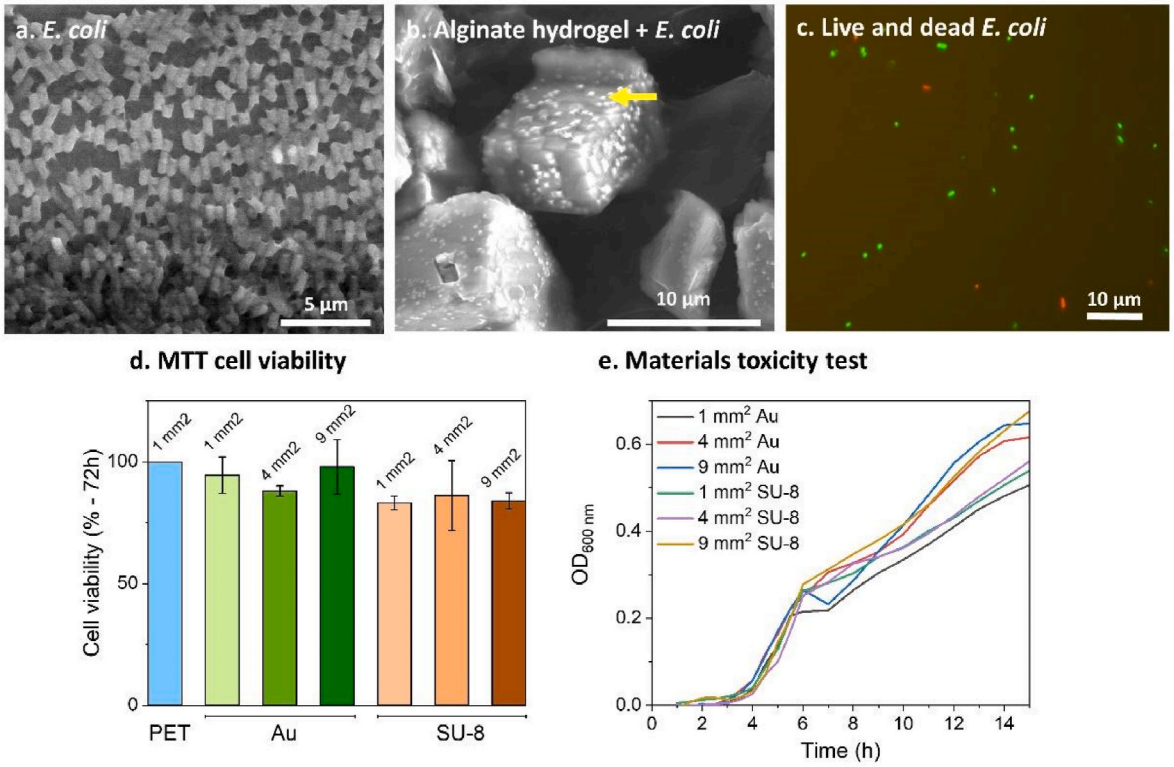

Fig. 4. LV-SEM images of (a) *E. coli* untreated cells and (b) bacteria retained in the 3D matrix of calcium alginate hydrogel with detail of $CaCO_3$ crystals. Yellow arrow points *E. coli* sitting on $CaCO_3$ crystals. (c) Live & dead test results images taken with a confocal microscope; where red are dead *E. coli* and in green are live *E. coli*. (d) MTT cell viability results after 72 h of incubation expressed in % (n = 3). (e) Toxicity test results of *E. coli* with Au and SU-8 in LB medium during 17 h.

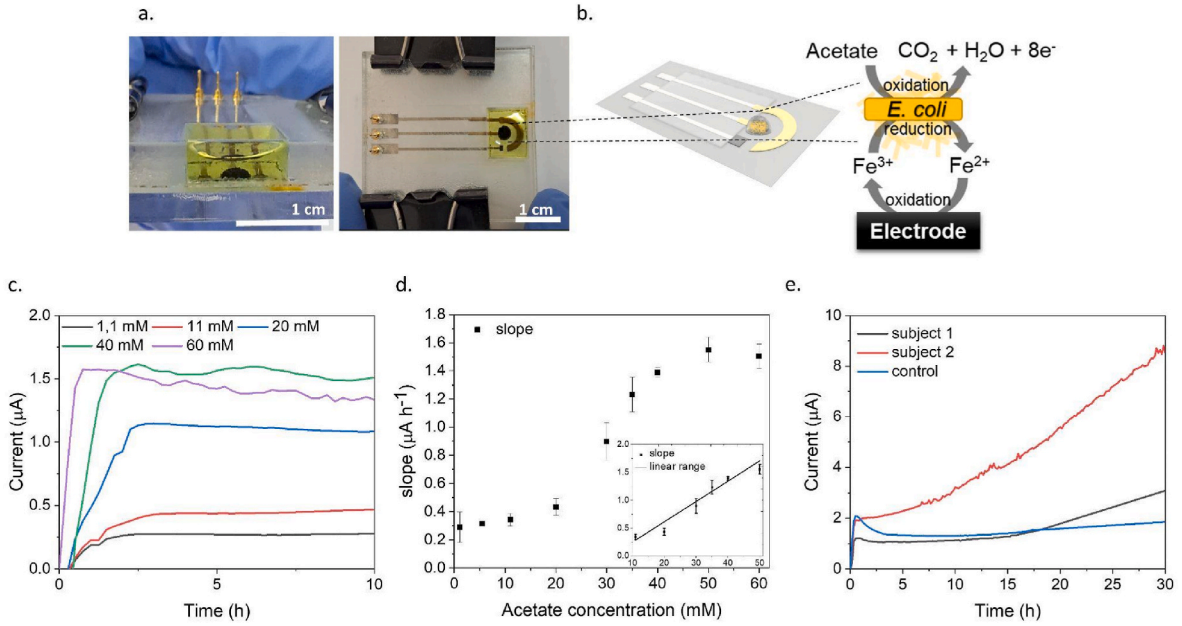

Fig. 5. (a) Picture of the side view (left) and the top view (right) of the 2 mm IJP sensor measuring set-up with the 3D conductive alginate hydrogel matrix encapsulating *E. coli*. (b) Left: scheme of the amperometric sensor with the bacterial conductive 3D-hydrogel matrix on top of the WE. Right: Schematic diagram of the mechanism of acetate determination by the *E. coli* biosensors in the presence of ferricyanide. (c) Time response chronoamperometry in presence of a mediator specimen (ferricyanide 10 M) for an acetate concentration of 1.1, 11, 20, 40, and 60 mM. The applied potential was 0.4 V *vs.* pseudo-Ag/AgCl. (d) Calibration curve of steady-state current response of *E. coli* bacteria immobilized in conductive alginate hydrogel to different acetate concentration *versus* the slope (n = 3; experimental error was calculated as standard deviation). (e) Time response chronoamperometry of the acetate biosensor to samples extracted from proximal zones of an in vitro colonic fermenter samples over 30 h, the control was performed with the same current measuring set up with the nutritional medium PDNM002B.

mm^2 IJP Au and SU-8 on PET were evaluated for being the WE and the passivation materials, respectively. PET substrates alone were also analysed and considered as controls for being a non-cytotoxic material. The samples were introduced in well plates containing MRC cells, and incubated under optimal proliferation conditions (DMEM medium supplemented with 10% PBS; pH = 7.2; T = 37 °C; 5% CO_2; 20% O_2) for 72 h. The MTT assay was then conducted to determine cellular metabolic activity after incubation, as an indicator of cell viability, proliferation and cytotoxicity. The colorimetric changes of the wells were studied at 570 nm, the maximum absorption band of the compound, and images of the materials in contact with the cells were taken 72 h after the incubation for completeness. MTT results are illustrated in Fig. 4d. As shown, both IJP materials presented low cytotoxic effects, with viability values always above 80%. There was no correlation between the amount of material and the cytotoxicity, and the difference between samples may be attributed to experimental variability between cultures and sample manipulation. It is important to highlight, both inks and printing technologies may be used to develop biosensors to monitor mammalian cells without being a risk for their integrity or function.

3.3. Electrochemical biosensor for determination of acetate concentration

For acetate detection, the redox mediator ferricyanide was used as indicator of bacterial metabolism of acetate. Experimentally, 200 μL of 10 mM ferricyanide solutions containing acetate concentrations in the range between 0 and 60 mM were introduced in the reservoir of the chamber, on top of the microbial biosensor as shown in Fig. 5a. Taking into account that ferricyanide serves as a mediator, a higher concentration of 10 mM was chosen in the electrochemical measurements to ensure that it was not limiting in the reactions taking place as the number of immobilized bacteria is increased up to 10^9 cfu and the experimental measurements were conducted over a long duration. Ferrocyanide production through bacterial metabolism was used to determine the acetate concentration by chronoamperometry at 0.4 V (*vs.* Ag/AgCl pseudo-RE). That is, *E. coli* metabolized acetate, oxidizing it to CO_2, and producing an electron flow in the electron transport chain. Ferricyanide reacted with the proteins and mediators in this chain, being reduced to ferrocyanide, which accumulated in the surroundings of the microbial biosensor over time. As shown in the schematic diagram illustrated in Fig. 5b, the ferrocyanide accumulation was then measured chronoamperometrically with the IJP-sensor, reporting on the initial concentration of acetate in the sample. The response of the sensor to ferrocyanide accumulation and thus, to acetate metabolism, is presented in Fig. 5c. Some differences between acetate concentrations were observed in the slope (μA h^{-1}) or rate of consumption of acetate of the chronoamperometric plot. As well as the current and the time necessary and the detection time, this is understood as the time necessary to reach a detectable concentration of ferrocyanide. From the three parameters, the slope of the curve was the one providing a better correlation with acetate concentration and was used here for acetate determination. In Fig. 5d, the variation of the slope magnitude with the acetate concentration is represented, showing a conventional sigmoidal curve with a detection limit of 3.6 mM (calculated with Sy/x/m criterion; where Sy/x is standard deviation of residuals and m is the slope of calibration curve), a linear range between 11 and 50 mM, and a sensitivity of 0.035 ± 0.004 μA h^{-1} mM^{-1}. Considering these merit figures, it may be concluded that this microbial biosensor configuration based on the metabolic activity of *E. coli* and employing IJP technology was suitable for acetate detection in a wide range of concentrations, although the sensitivity and detection range should be adjusted to be useful in the monitoring of acetate in GOC systems.

Conventional techniques such as Liquid chromatography (LC), Ion Exclusion Chromatography (IEC) and Metabolomic technique (MT), are widely recognized as powerful and reliable techniques for analytical purposes, especially achieving high accuracy and sensitivity in the measurements of all SCFAs (see Table 1). However, they all require sophisticated and complex equipment, skilled operators, and time-consuming sample preparation steps, which can be costly and which makes it difficult to downsize them for integration into portable or miniaturized platforms. While these methods provide accurate analysis, there are certain drawbacks. LC, in particular, has a longer response time due to the separation of compounds, sometimes taking hours or even days to complete. In contrast, IEC and MT offer faster results, saving time in the analysis process.

Recently, emerging sensing technologies such as electrochemical biosensors, microbial sensors, and fuel cells offer more promise in the miniaturization field. Their simplified design, ease of operation, and simple equipment make them attractive candidates for miniaturized systems and integration into portable systems. These sensors demonstrate the ability to rapidly monitor signals associated with SCFAs. Among them, our electrochemical biosensor has a medium-long response time of a few hours. One advantage of both the anaerobic fuel cell and our electrochemical biosensor is their potential integration into analysis systems. Moreover, these sensors do not require specific, expensive equipment, making them more cost-effective. Additionally, our proposed biosensor can operate in aerobic conditions, which enhances its user-friendliness and adaptability.

Overall, while conventional techniques like LC, IEC, and MT have their strengths in terms of accuracy and comprehensive analysis, their integration into miniaturized systems remains a challenge. Alternatively, sensor-based approaches show great potential for portable and miniaturized SCFAs measurements.

3.4. Determination of acetate concentration in vitro colonic fermenters

The colonic microbiota metabolism includes the production of SCFAs, mainly acetate, propionate, and butyrate, produced by anaerobic bacteria due to the fermentation of non-digestible fibers. The bacteria responsible for the production of most of the SCFAs are *Eubacterium*, *Faecalibacterium*, *Ruminnococus,* and *Roseburia* genera (*Firmicutes phylum*) and also many species from the *Bacteroidota phylum*. The relative proportions of acetate, propionate, and butyrate vary with diet and age but typically are 3:1:1 [36] However, the chromatography results showed that the samples used in this study had an increased proportion of butyrate (Table 2). This increase in butyrate, which is considered as anti-inflammatory SCFA, is probably due to the in vitro treatment of

Table 1
Comparison acetate detection techniques.

Acetate detection	Linear Range (mM)	Monitoring	Response time[b]	Integration	Cost	aerobic/anaerobic	REF
Liquid chromatography	0.001–60[a]	no	moderate -long	no	high	aerobic & anaerobic	[8]
Ion exclusion chromatography	0.002–0.06[a]	no	short- moderate	no	high	aerobic & anaerobic	[9]
Metabolomic technique	0.01–6.1	no	short- moderate	no	high	aerobic & anaerobic	[10]
Anaerobic fuel cell	<0.48	yes	short	yes	low	anaerobic	[19]
Bio-electrolytic sensor	5–100	yes	short	no	medium	anaerobic	[20]
Amperometric microbial microsensor	0–1.6	yes	short	no	medium	anaerobic	[21]
Electrochemical biosensor	11–50	yes	moderate- long	yes	low	aerobic	This work

[a] The linear range could probably be extended to higher concentrations.
[b] Long (hours to days), Moderate (minutes to hours), Short (seconds to minutes).

Table 2
Concentration of SCFA (mM) at the proximal zone of samples extracted from an in vitro colonic fermenter measured with chromatography and with the electrochemical biosensor (n = 2).

	Short-Chain Fatty Acids by Chromatography			Electrochemical Biosensor
Sample	Butyrate	Propionate	Acetate	Acetate
Subject 1	23,91	4.50	22,21	7.4 ± 0.8
Subject 2	24,27	7.90	27,90	11.8 ± 0.7

colonic microbiota with the probiotic (*Bifidobacterium animalis*). Differences among subjects can be explained by the fact that the fecal inoculums for the in vitro fermentation study were obtained from different subjects presenting different characteristics, thus assuming that baseline microbiota differed. The type of diet, genetics, or environmental factors can shape the microbiota composition of each subject and hence the response to the probiotic treatment and the metabolites found in their colonic medium.

In Fig. 5e, the time response of our sensor to these samples is presented in the form of chronoamperometry over 30 h. The microbial biosensor exhibited two distinct slopes associated with the bacterial metabolism of two separate carbon sources. The initial sharp slope corresponded to the rapid consumption of a highly efficient carbon source, likely glucose. The control experiment performed with the nutritional medium PDNM002B and the same current measuring set up clearly indicates the presence of this carbon source. The subsequent smaller slope indicated the utilization of a less energetically favorable substrate, specifically acetate. Considering the composition of the samples and the selectivity of the microbial biosensor (which is more sensitive to acetate than other SCFAs such as butyrate or propionate), the second slope was associated for determining the acetate concentration in the samples by interpolation on the previously established calibration curve. When comparing the quantified values obtained through HPLC and amperometric biosensing (two replicates, n = 2) notable discrepancies were observed. While both systems exhibited similar tendencies (subject 2 with higher acetate concentrations than subject 1), the values obtained with the biosensor were significantly lower. Specifically, subject 1 had acetate concentrations of 22.21 mM by HPLC and 7.4 ± 0.8 mM by the biosensor, while subject 2 had concentrations of 27.90 mM by HPLC and 11.8 ± 0.7 mM by the biosensor. Despite this discrepancy, the relative relationship between the two subjects remains consistent. Subject 2 exhibits approximately 25% higher acetate concentration compared to subject 1, as observed in the HPLC results. Similarly, the biosensor readings also show a similar trend, with subject 2 displaying approximately 22% higher acetate concentration compared to subject 1. However, this disparity can be attributed to various factors. Firstly, the quantification method involves interpolating real sample values onto a calibration curve generated with spiked buffer samples. In addition to inherent composition differences that can introduce matrix effects during amperometric measurements, other factors such as pH (pH of our calibration curve is done approximately at pH 7, the control and the real samples of the proximal reactor are around pH 6), conductivity of the medium, or the presence of potential inhibitory substances that can impact bacterial metabolism may have influenced acetate determination, thereby compromising the precision of the biosensor. It is important to carefully consider these factors and perform further investigations in the future such as recalibration of the sensor using spiked samples prepared under identical matrix conditions and experimental parameters (pH, conductivity, etc.) to establish the precise reasons for the differences observed in the acetate concentrations measured by the two methods.

5. Conclusions

In the work, a microbial biosensor based on biocompatible material and technologies has been developed for the detection of acetate in aerobic conditions. Custom-made inkjet printed transducers have been used for biosensor development for their simplicity, miniaturization potential, low cost and compatibility with the fabrication of most advanced organ-on-a-chip system or to be integrated in colonic in vitro fermentation systems. *E. coli* bacteria were immobilized on the surface of Au IJP electrodes by electrodeposition of conductive alginate hydrogels, which provide a high control on the deposition area, repeatability and the possibility to immobilize high bacterial concentrations without compromising their viability and function. Bacterial metabolism of *E. coli* results selective in acetate oxidation, while exhibiting an inability to metabolize both butyrate or propionate. This metabolic process leads to the production of an electron flow through the electron transport chain that can be detected with an electrochemical biosensor, this case thanks to the use of ferricyanide as redox mediator. Thus, metabolic reduction of ferricyanide to ferrocyanide associated to acetate metabolism in aerobic conditions can be detected with the sensor, reporting on acetate concentration in the range between 11 mM and 50 mM, with a sensitivity of 0.035 ± 0.004 μA h^{-1} mM^{-1}. Proximal samples of an in vitro colonic fermenter were successfully monitored during 30 h, revealing the presence of two distinct carbon sources. The second carbon source, which was associated with acetate as a less energetically favorable substrate, enabled the determination of its concentration. The relative relationship between the two subjects, as determined by the biosensor, remained consistent and aligned with the findings from the chromatographic analysis. The hydrogel demonstrated excellent stability, maintaining its integrity and strong adherence to the electrode for up to 72 h. The viability of *E. coli* within the hydrogel decreased by one order of magnitude after 24 h of storage in PBS and two orders of magnitude when stored in glucose. Despite this decrease in bacterial survival, the hydrogel remained stable and capable of recording acetate for nearly 30 h without compromising its performance. The reported immobilized approach is an interesting result of exploiting bacteria as a biosensor tool.

Credit author statement

E. Forner: Investigation, Methodology, Writing – original draft. J. J. Ezenarro: Methodology, Software, Visualization. M. Pérez-Montero: Methodology. N. Vigués: Methodology. A. Asensio-Grau: Methodology. A. Andrés: Conceptualization. J. Mas: Resources. M. Baeza: Methodology. X. Muñoz-Berbel: Conceptualization, Methodology, Writing – review & editing. R. Villa: Funding acquisition, Project administration; Resources. G. Gabriel: Conceptualization, Methodology, Investigation, Visualization, Writing – review & editing, Supervision.

Declaration of competing interest

The authors declare that they have no known competing financial interests or personal relationships that could have appeared to influence the work reported in this paper.

Data availability

Data will be made available on request.

Acknowledgements

The authors acknowledge the support from the Ministerio de Ciencia Innovacion y Universidades (MICIU/FEDER, EU), in Spain, through GUMICHIP (RTI2018-096786-B-I00), GALILEI (PID2021-126253OB-C21) and CHIP4CELL projects (PID2021-127653NB-C21) and the support of the Generalitat de Catalunya to 2021SGR00495. The work has been performed by the ICTS "NANBIOSIS", more specifically by the U8 Unit of the CIBER in Bioengineering, Biomaterials & Nanomedicine (CIBER-BBN) at the IMB-CNM (CSIC). This work also made use of the

Spanish ICTS Network MICRONANOFABS partially supported by MEINCOM. We would like to thank the members of the GENOCOV research group from Universitat Autonoma, specifically Dr. D. Gabriel and PhD student M. Fachal, for their assistance in the liquid chromatography analysis presented in this work.

Appendix A. Supplementary data

Supplementary data to this article can be found online at https://doi.org/10.1016/j.talanta.2023.124882.

References

[1] M. Levy, C.A. Thaiss, E. Elinav, Metabolites: Messengers between the Microbiota and the Immune System, 2016, https://doi.org/10.1101/gad.284091.
[2] M.F. Neurath, Host–microbiota interactions in inflammatory bowel disease, Nat. Rev. Gastroenterol. Hepatol. 17 (2020) 76–77, https://doi.org/10.1038/s41575-019-0248-1.
[3] K.E.B. Knudsen, H.N. Lærke, M.S. Hedemann, T.S. Nielsen, A.K. Ingerslev, D.S. G. Nielsen, P.K. Theil, S. Purup, S. Hald, A.G. Schioldan, M.L. Marco, S. Gregersen, K. Hermansen, Impact of diet-modulated butyrate production on intestinal barrier function and inflammation, Nutrients 10 (2018), https://doi.org/10.3390/nu10101499.
[4] E.S. Chambers, T. Preston, G. Frost, D.J. Morrison, Role of gut microbiota-generated short-chain fatty acids in metabolic and cardiovascular health, Curr Nutr Rep 7 (2018) 198–206, https://doi.org/10.1007/s13668-018-0248-8.
[5] D. Salamone, A.A. Rivellese, C. Vetrani, The relationship between gut microbiota, short-chain fatty acids and type 2 diabetes mellitus: the possible role of dietary fibre, Acta Diabetol. 58 (2021) 1131–1138, https://doi.org/10.1007/s00592-021-01727-5.
[6] Y.P. Silva, A. Bernardi, R.L. Frozza, The role of short-chain fatty acids from gut microbiota in gut-brain communication, Front. Endocrinol. 11 (2020), https://doi.org/10.3389/fendo.2020.00025.
[7] D.J. Morrison, T. Preston, Formation of short chain fatty acids by the gut microbiota and their impact on human metabolism, Gut Microb. 7 (2016) 189–200, https://doi.org/10.1080/19490976.2015.1134082.
[8] L.R. Hoving, M. Heijink, V. van Harmelen, K.W. van Dijk, M. Giera, GC-MS analysis of short-chain fatty acids in feces, cecum content, and blood samples, in: Methods in Molecular Biology, Humana Press Inc., 2018, pp. 247–256, https://doi.org/10.1007/978-1-4939-7592-1_17.
[9] M. Bertges, J. van Helden, R. Weiskirchen, Quantification of Short Chain Fatty Acids (acetate, butyrate, propionate) in human blood with ion exclusion chromatography, Pract Lab Med 26 (2021), https://doi.org/10.1016/j.plabm.2021.e00244.
[10] M. Primec, D. Mičetić-Turk, T. Langerholc, Analysis of short-chain fatty acids in human feces: a scoping review, Anal. Biochem. 526 (2017) 9–21, https://doi.org/10.1016/j.ab.2017.03.007.
[11] J. Isenring, L. Bircher, A. Geirnaert, C. Lacroix, In vitro human gut microbiota fermentation models: opportunities, challenges, and pitfalls, Microbiome Research Reports 2 (2023) 2, https://doi.org/10.20517/mrr.2022.15.
[12] D. Dupont, M. Alric, S. Blanquet-Diot, G. Bornhorst, C. Cueva, A. Deglaire, S. Denis, M. Ferrua, R. Havenaar, J. Lelieveld, A.R. Mackie, M. Marzorati, O. Menard, M. Minekus, B. Miralles, I. Recio, P. Van den Abbeele, Can dynamic in vitro digestion systems mimic the physiological reality? Crit. Rev. Food Sci. Nutr. 59 (2019) 1546–1562, https://doi.org/10.1080/10408398.2017.1421900.
[13] E. Veintimilla-Gozalbo, A. Asensio-Grau, J. Calvo-Lerma, A. Heredia, A. Andrés, Vitro Simulation of Human Colonic Fermentation: A Practical Approach towards Models' Design and Analytical Tools, 2021, https://doi.org/10.3390/app.
[14] L. Amirifar, A. Shamloo, R. Nasiri, N.R. de Barros, Z.Z. Wang, B.D. Unluturk, A. Libanori, O. Ievglevskyi, S.E. Diltemiz, S. Sances, I. Balasingham, S.K. Seidlits, N. Ashammakhi, Brain-on-a-chip: recent advances in design and techniques for microfluidic models of the brain in health and disease, Biomaterials 285 (2022), https://doi.org/10.1016/j.biomaterials.2022.121531.
[15] J. Deng, W. Wei, Z. Chen, B. Lin, W. Zhao, Y. Luo, X. Zhang, Engineered liver-on-a-chip platform to mimic liver functions and its biomedical applications: a review, Micromachines 10 (2019), https://doi.org/10.3390/mi10100676.
[16] Claudio Franco, Holger Gerhardt, Blood vessels on a chip, Nature 488 (2012) 465–466.
[17] S.N. Bhatia, D.E. Ingber, Microfluidic organs-on-chips, Nat. Biotechnol. 32 (2014) 760–772, https://doi.org/10.1038/nbt.2989.
[18] M. Trapecar, C. Communal, J. Velazquez, C.A. Maass, Y.J. Huang, K. Schneider, C. W. Wright, V. Butty, G. Eng, O. Yilmaz, D. Trumper, L.G. Griffith, Gut-Liver physiomimetics reveal paradoxical modulation of IBD-related inflammation by short-chain fatty acids, Cell Syst 10 (2020) 223–239.e9, https://doi.org/10.1016/j.cels.2020.02.008.
[19] A. Kaur, J.R. Kim, I. Michie, R.M. Dinsdale, A.J. Guwy, G.C. Premier, Microbial fuel cell type biosensor for specific volatile fatty acids using acclimated bacterial communities, Biosens. Bioelectron. 47 (2013) 50–55, https://doi.org/10.1016/j.bios.2013.02.033.
[20] X. Jin, X. Li, N. Zhao, I. Angelidaki, Y. Zhang, Bio-electrolytic sensor for rapid monitoring of volatile fatty acids in anaerobic digestion process, Water Res. 111 (2017) 74–80, https://doi.org/10.1016/j.watres.2016.12.045.
[21] E. Atci, J.T. Babauta, S.T. Sultana, H. Beyenal, Microbiosensor for the detection of acetate in electrode-respiring biofilms, Biosens. Bioelectron. 81 (2016) 517–523, https://doi.org/10.1016/j.bios.2016.03.027.
[22] E. Atci, J.T. Babauta, P.T. Ha, H. Beyenal, A fumarate microbiosensor for use in biofilms, J. Electrochem. Soc. 164 (2017) H3058–H3064, https://doi.org/10.1149/2.0101703jes.
[23] Y.F. Wang, S.S. Cheng, S. Tsujimura, T. Ikeda, K. Kano, Escherichia coli-catalyzed bioelectrochemical oxidation of acetate in the presence of mediators, Bioelectrochemistry 69 (2006) 74–81, https://doi.org/10.1016/j.bioelechem.2005.11.003.
[24] J. Muñoz, L.J. Brennan, F. Céspedes, Y.K. Gun'ko, M. Baeza, Characterization protocol to improve the electroanalytical response of graphene-polymer nanocomposite sensors, Compos. Sci. Technol. 125 (2016) 71–79, https://doi.org/10.1016/j.compscitech.2016.01.018.
[25] A. Márquez, C. Jiménez-Jorquera, C. Domínguez, X. Muñoz-Berbel, Electrodepositable alginate membranes for enzymatic sensors: an amperometric glucose biosensor for whole blood analysis, Biosens. Bioelectron. 97 (2017) 136–142, https://doi.org/10.1016/j.bios.2017.05.051.
[26] N. Vigués, F. Pujol-Vila, A. Marquez-Maqueda, X. Muñoz-Berbel, J. Mas, Electro-addressable conductive alginate hydrogel for bacterial trapping and general toxicity determination, Anal. Chim. Acta 1036 (2018) 115–120, https://doi.org/10.1016/j.aca.2018.06.062.
[27] P. Van Den Abbeele, C. Grootaert, M. Marzorati, S. Possemiers, W. Verstraete, P. Gérard, S. Rabot, A. Bruneau, S. Aidy Ei, M. Derrien, E. Zoetendal, M. Kleerebezem, H. Smidt, T. Van De Wiele, Microbial community development in a dynamic gut model is reproducible, colon region specific, and selective for bacteroidetes and Clostridium cluster IX, Appl. Environ. Microbiol. 76 (2010) 5237–5246, https://doi.org/10.1128/AEM.00759-10.
[28] F. Bianchi, N. Larsen, T. de Mello Tieghi, M.A.T. Adorno, W. Kot, S.M.I. Saad, L. Jespersen, K. Sivieri, Modulation of gut microbiota from obese individuals by in vitro fermentation of citrus pectin in combination with Bifidobacterium longum BB-46, Appl. Microbiol. Biotechnol. 102 (2018) 8827–8840, https://doi.org/10.1007/s00253-018-9234-8.
[29] A. Bren, J.O. Park, B.D. Towbin, E. Dekel, J.D. Rabinowitz, U. Alon, Glucose becomes one of the worst carbon sources for E.coli on poor nitrogen sources due to suboptimal levels of cAMP, Sci. Rep. 6 (2016), https://doi.org/10.1038/srep24834.
[30] J. Monod, Recherches sur la croissance des cultures bacteriennes, Ann. Inst. Pasteur vol. 69, 1942.
[31] B.T. Layden, A.R. Angueira, M. Brodsky, V. Durai, W.L. Lowe, Short chain fatty acids and their receptors: new metabolic targets, Transl. Res. 161 (2013) 131–140, https://doi.org/10.1016/j.trsl.2012.10.007.
[32] S. Štumpf, G. Hostnik, M. Primožič, M. Leitgeb, U. Bren, Generation times of E. coli prolong with increasing tannin concentration while the lag phase extends exponentially, Plants 9 (2020) 1–11, https://doi.org/10.3390/plants9121680.
[33] F. Pujol-Vila, N. Vigués, M. Díaz-González, X. Muñoz-Berbel, J. Mas, Fast and sensitive optical toxicity bioassay based on dual wavelength analysis of bacterial ferricyanide reduction kinetics, Biosens. Bioelectron. 67 (2015) 272–279, https://doi.org/10.1016/j.bios.2014.08.030.
[34] F. Pujol-Vila, N. Vigués, A. Guerrero-Navarro, S. Jiménez, D. Gómez, M. Fernández, J. Bori, B. Vallès, M.C. Riva, X. Muñoz-Berbel, J. Mas, Paper-based chromatic toxicity bioassay by analysis of bacterial ferricyanide reduction, Anal. Chim. Acta 910 (2016) 60–67, https://doi.org/10.1016/j.aca.2016.01.006.
[35] Hans Bremer, Variation of Generation Times in Escherichia coli Populations: its Cause and Implications, 1982.
[36] J. Ghyselinck, L. Verstrepen, F. Moens, P. Van den Abbeele, J. Said, B. Smith, I. Bjarnason, A.W. Basit, S. Gaisford, A 4-strain probiotic supplement influences gut microbiota composition and gut wall function in patients with ulcerative colitis, Int. J. Pharm. 587 (2020), https://doi.org/10.1016/j.ijpharm.2020.119648.